Traveling-Wave Maser Experiments Using Ruby at *X* Band

G. I. HADDAD, MEMBER, IEEE, AND D. H. PAXMAN

Summary—**The characteristics of a traveling-wave maser using ruby and a Karp-type slow-wave structure in the *X*-band frequency range are presented. Several possible operating points in ruby in this frequency range were examined and the inversion ratio, linewidth, paramagnetic absorption, and electronic gain at these points were measured. The experimental results are compared with the theoretical predictions. The problems involved in the design of the traveling-wave maser are discussed and the performance that may be expected of a maser using good ruby crystals, a well matched structure, and sufficient pump power is evaluated. Experimental results on YIG slabs employed in the maser for isolation are presented and compared with theoretical predictions.**

I. Introduction

THE ADVANTAGES and theory of operation of the traveling-wave maser have been discussed in detailed in the literature [1]. Due to the desirable characteristics that can be obtained in such a maser as compared to the earlier cavity ones, several traveling-wave masers have been built and studied at different laboratories [1]–[5]. Most of these traveling-wave masers have operated, however, at frequencies of 6 Gc and lower. An *X*-band coupled cavity transmission maser [6] and a millimeter traveling-wave maser have been recently described in the literature [7].

An *X*-band traveling-wave maser was built at this laboratory a few years ago and was described elsewhere [5]. It was felt, however, that the results on this maser were rather incomplete; some further experiments were recently performed, and a greatly improved performance has been achieved.

The purpose of this report is to describe the results of these experiments and to compare the experimental results with the theoretical predictions. Several possible operating points in the *X*-band frequency range using ruby as the active maser material were investigated in a Karp-type slow-wave structure. The linewidth, inversion, absorption, and electronic gain at these different points were measured and the advantages and disadvantages of utilizing either of these points in a traveling-wave maser are discussed.

II. Design Considerations

The gain in a traveling-wave maser may be expressed as [1]

$$G_{\mathrm{db}} = 27.3 \frac{SNFI}{Q_{m(\mathrm{abs.})}} \tag{1}$$

where

S = slowing factor = c/v_g
N = the active length of the structure expressed in free-space wavelengths
F = filling factor
$Q_{m(\mathrm{abs.})}$ = the absorption magnetic Q of the paramagnetic material
I = the inversion ratio.

S, N, and F in the above equation depend on the slow-wave structure. $Q_{m(\mathrm{abs.})}$ depends on the paramagnetic material, the orientation of the material in the structure and the operating point. The degree of inversion depends on the operating point. The slow-wave structure and the paramagnetic material employed in these experiments are discussed in the following sections.

A. Slow-Wave Structure

The slow-wave structure that was employed in these experiments is a double-ridge Karp-type configuration. The essential features of this structure as employed in a traveling-wave maser have been presented elsewhere [5]. The dispersion characteristics of the structure when loaded with a dielectric material may be predicted closely by a space-harmonic analysis. Such an analysis has been performed and the results obtained from it appear in detail elsewhere [8].

It is believed that this structure offers several advantages over other slow-wave structures which have been employed in traveling-wave masers, especially at the higher frequencies. These advantages are discussed in detail elsewhere [8] and are only mentioned here briefly. They include mechanical rigidity, ease of fabrication, higher saturation power outputs, and size.

Cross sections of the slow-wave structure that was employed in these experiments are shown in Fig. 1. The location and orientation of the paramagnetic material and the isolating material in the structure are also shown. The structure pass band was approximately 900 Mc wide and extended from 8 to 8.9 Gc. The ω-β characteristic and the slowing factor across the band are shown in Fig. 2.

The RF fields will have different senses of polarization above and below the ladder line. The direction of the RF magnetic fields relative to the c axis of the ruby has a great effect on the magnetic Q. An approximate

Manuscript received January 6, 1964; revised March 16, 1964, This work was supported by the Electronic Technology Laboratory, Aeronautical Systems Division, under Contract AF-33(657)-8050.

The authors are with Electron Physics Laboratory, Department of Electrical Engineering, The University of Michigan, Ann Arbor, Mich.

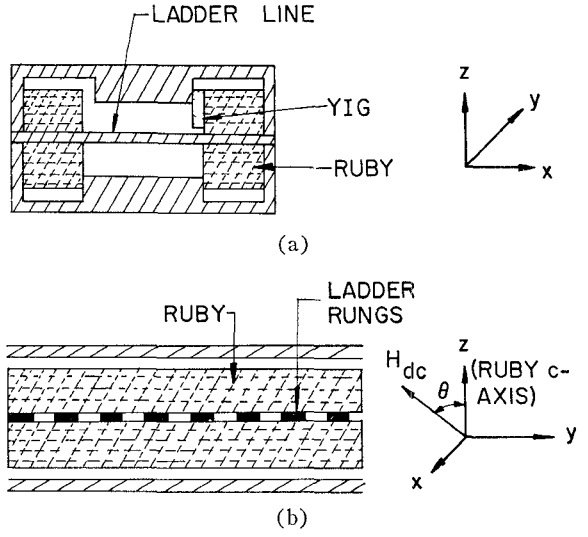

Fig. 1—Cross sections of TWM structure.

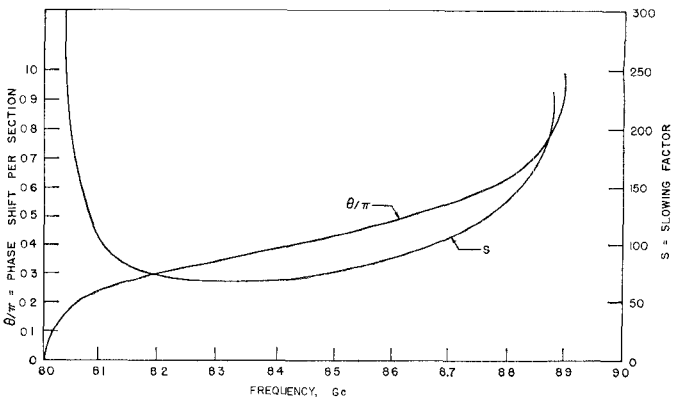

Fig. 2—ω-β characteristic and the slowing factor for the loaded structure.

qualitative understanding of the degree of ellipticity of the magnetic fields at different points in the pass band is facilitated by considering currents flowing in the tapes. It can then be deduced that the RF fields are approximately linearly polarized in the y direction at the lower cutoff frequency. As the frequency is increased the fields become elliptically polarized with $h_y > h_z$ until the middle of the pass band is reached where the fields become circularly polarized. As the frequency is increased further the fields become again elliptically polarized with $h_z > h_y$. When the upper cutoff frequency is reached, the fields again become linearly polarized, but in the z direction.

The other factor in the gain equation which depends on the structure is the filling factor. The RF fields fall off in the z direction, away from the structure, as $e^{-j\beta z}$. This, of course, results in a higher filling factor at the lower frequency end of the pass band where β is smaller than at the higher frequency end. The tape thickness in this structure is very small, however, which will tend to de-emphasize this difference. However, the fields still become more concentrated at the higher frequency end, which tends to decrease the saturation power output of the maser at those frequencies.

B. Paramagnetic Material

The paramagnetic material that was employed in these experiments was Linde pink ruby with a Cr^{3+} concentration specified by the supplier as 0.05 per cent. The absorption magnetic Q which appears in the gain expression depends on the operating point and orientation of the c axis with respect to the RF fields in the slow-wave structure. The inversion ratio depends on the operating point. Three typical operating points in the X-band frequency range are shown in Fig. 3. These are

1) $\theta = 90°$ high-field point. Two possible modes of operation exist here. In the first the pump power is applied between levels 1 and 3 while in the second the pump power is applied between levels 1 and 4, the signal frequency being the same, namely between levels 1 and 2.
2) $\theta = 54.7°$ or the push-pull point [9]. Here the energy separation between levels 1 and 3 and 2 and 4 is the same and a single pump frequency may be employed to saturate these levels. The signal frequency is that between levels 2 and 3.
3) $\theta = 90°$ low-field point [10]. Here, operation at a pump frequency lower than the signal frequency can be achieved.

Only the first two points were experimentally investigated here. The third point is quite unfavorable for a traveling-wave maser operation compared with the other points. The reason is that the measured inversion ratio at this point is quite low [10] (0.37) and the absorption magnetic Q is generally higher at this point than at the other points (Figs. 4 and 5).

The absorption magnetic Q of the material may be expressed in general as

$$Q_{m(\text{abs.})} = \frac{2kT\Delta f}{\pi N_0 g^2 \beta^2 f_s [(\phi_1 \alpha_r + \phi_3 \gamma_r) \pm \phi_2 \beta_i]^2} \tag{2}$$

where

N_0 = the number of paramagnetic ions per cm^3
g = the spectroscopic splitting factor
β = the Bohr magneton
f_s = the signal frequency
k = Boltzmann's constant
T = the temperature, °K
Δf = the linewidth of the signal transition
ϕ_1, ϕ_2, ϕ_3 = the direction cosines of the RF magnetic field [11]
$\alpha_r, \gamma_r, \beta_i$ = the elements of the transition matrix [11].

The double sign in the above expression refers to different senses of polarization of the RF fields.

It can be seen by referring to Fig. 1, where the orientation of the dc magnetic field and the ruby in the slow-wave structure are shown, that ϕ_1 in this case is zero.

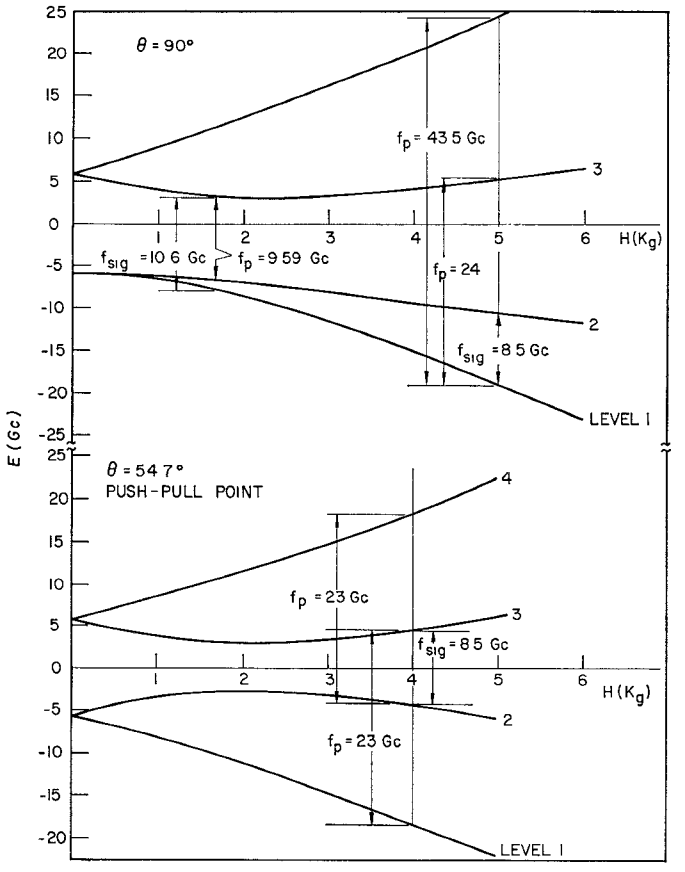

Fig. 3—Energy level diagrams for ruby.

For circularly polarized RF fields, (2) reduces to

$$Q_{m(\text{abs.})} = \frac{4kT\Delta f}{\pi N_0 g^2 \beta^2 f_s [\gamma_r \pm \beta_i]^2}. \tag{3}$$

α_r, γ_r and β_i which appear in the above expressions have been computed and appear elsewhere [11]. The only unknowns in the above expression are then the linewidth and the concentration. The linewidth was measured at the different operating points and from this an estimate of the concentration may be obtained [12].

1) Linewidth Measurements: The linewidth of the ruby material which was employed in these experiments was measured. A small sample was placed in a cavity and a slow field sweep, together with 1 kc/sec modulation was employed. This enables the derivative of the line shape to be displayed on an x-y recorder where the x direction is driven by a precision resistor placed in the magnet supply lead. An N.M.R. magnetometer was used to calibrate the x-direction displacement. The full displacement in this case was approximately 300 gauss.

The method gave the width, in gauss, of the points of maximum slope on the absorption curve which was converted to the width at the half power points through multiplication by a correction factor. Assuming a Gaussian line shape [13] in this concentration region the correction factor is 1.175.

In order to express the linewidth in megacycles, the slope of the frequency separation between the two

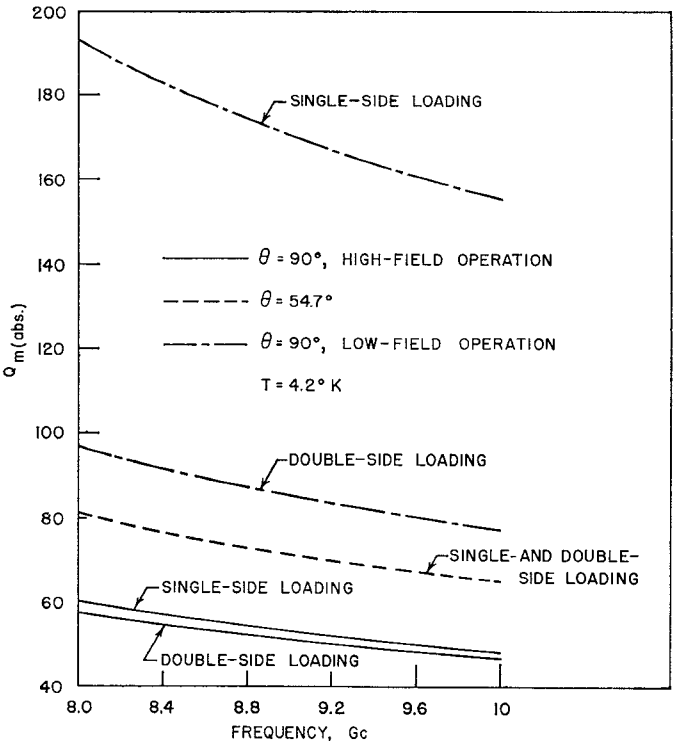

Fig. 4—$Q_{m(\text{abs.})}$ vs frequency for single- and double-side loading at different operating points for circularly polarized RF fields.

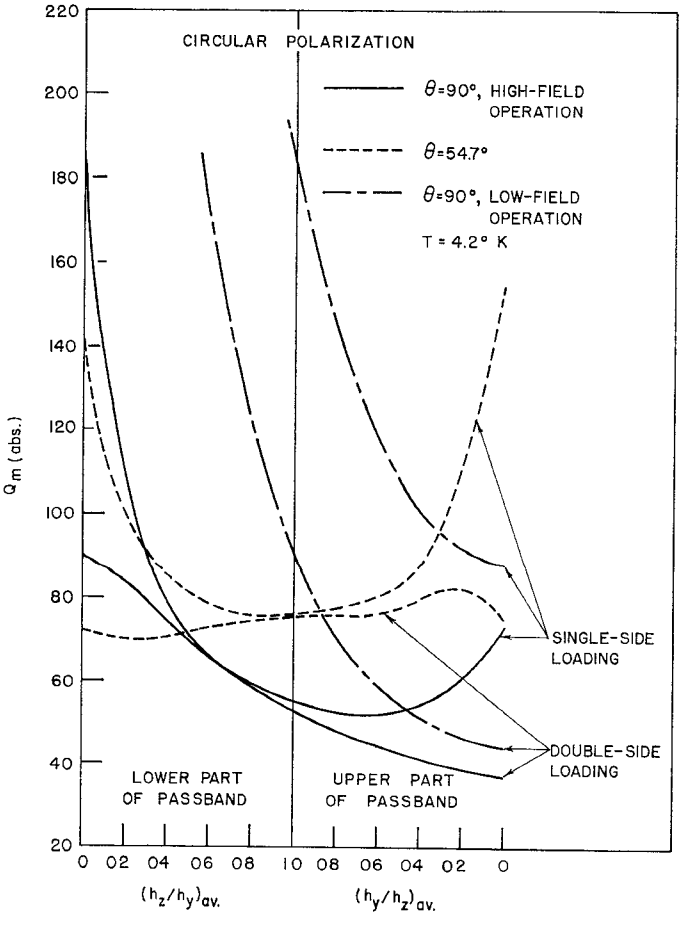

Fig. 5—$Q_{m(\text{abs})}$ vs RF field ellipticity (f_{signal}=8.5 Gc).

pertinent levels was obtained from Chang and Siegman [11] where for $\theta = 54.7°$ the slope was estimated as 2.92 Mc/gauss and for $\theta = 90°$ (high field point) as 2.625 Mg/gauss. The results are given in Table I.

TABLE I
LINEWIDTH

θ	T	Δf
90°	290°K	61 Mc
54.7°	290°K	82 Mc

The dependence of linewidth on concentration has been given elsewhere [12]. Comparison with this data showed that the concentration was 0.045 per cent (per cent Cr^{3+} to Al^{3+}) which is close to the manufacturer's estimate of 0.05 per cent. In view of the slow variation of the linewidth with concentration in this region this value is regarded as approximate.

2) *Calculation of* $Q_{m(\text{abs.})}$: All the terms which are required to calculate Q_m are now determined and thus an estimate of Q_m may be obtained. This is shown in Figs. 4 and 5.

Fig. 4 shows $Q_{m(\text{abs.})}$ as a function of frequency for both double- and single-side loading[1] at the different operating points. In this figure the RF fields are assumed to be circularly polarized. For the $\theta = 90°$ high-field operation and $\theta = 54.7°$, the ruby orientation is that shown in Fig. 1 where the ruby c axis is perpendicular to the plane of the ladder tapes. For the $\theta = 90°$ low-field operation the ruby c axis is assumed to be parallel to the ladder tapes, since this orientation results in a much lower $Q_{m(\text{abs.})}$ than the first.

The magnetic Q for single- and double-side loading indicates the behavior of the transition matrix elements. For the $\theta = 54.7°$ point γ_r and β_i are equal and thus no improvement would be expected through double-side loading for circularly polarized RF fields. For the $\theta = 90°$ high-field point the difference between γ_r and β_i is very small and thus very little is gained through double-side loading. For the $\theta = 90°$, low-field point, $\alpha_r \gg \beta_i$, and thus the magnetic Q for double-side loading is reduced approximately to half its value for single-side loading.

Since the ellipticity of the RF fields varies across the pass band of the structure, the effect of this variation on the magnetic Q is shown in Fig. 5. It can be seen from this figure that for a double-side loaded structure the magnetic Q for the push-pull point is approximately constant with variations in the ellipticity of the RF fields. For the other two points the magnetic Q varies considerably with RF field ellipticity and is smallest for RF fields linearly polarized in the z direction.

[1] Double-side loading refers to the case in which the maser material is placed above and below the ladder line and single-side loading to the case when the maser material is placed on one side of the ladder line only.

3) *Theoretical Inversion Ratio:* The inversion ratio I is defined as

$$I = \frac{\Delta n_{ji \text{ pump on}}}{\Delta n_{ij \text{ pump off}}} \tag{4}$$

where Δn is the population difference between the pertinent levels.

The theoretical inversion ratio at the different operating points is given below.

a) $\theta = 90°$ *High Field Operation:* The inversion ratio at this point can be expressed as

$$I = \left(\frac{w_i}{w_i + w_s}\right)\frac{f_p}{f_s} - 1 \tag{5}$$

where

w_i, w_s = the thermal relaxation transition probabilities of the idler and signal transitions, respectively

f_p, f_s = the pump and signal frequencies, respectively.

The ideal case occurs when the idler relaxation time is zero ($w_i = \infty$) or when the signal relaxation time is infinite ($w_s = 0$). For this case I becomes

$$I = \frac{f_p}{f_s} - 1. \tag{6}$$

For equal relaxation times, I becomes

$$I = \frac{f_p}{2f_s} - 1. \tag{7}$$

b) $\theta = 54.7°$, *Push-Pull Point:* The inversion ratio at this point may be expressed as

$$I = \left[\frac{2w_{41} + w_{43} + w_{21}}{w_{41} + w_{43} + w_{21} + w_{32}}\right]\frac{f_p}{f_s} - 1. \tag{8}$$

The ideal case occurs when the relaxation time between levels 4 and 1 is zero ($w_{41} = \infty$) in which case I becomes

$$I = \frac{2f_p}{f_s} - 1. \tag{9}$$

It is then seen that for this ideal case, operation at pump frequencies lower than the signal frequency may be obtained, *i.e.*, $I > 0$ for $f_p \geqq f_s/2$.

For equal relaxation times between all levels I becomes

$$I = \frac{f_p}{f_s} - 1. \tag{10}$$

4) *Inversion Ratio Measurements:* The inversion ratio was measured at the $\theta = 90°$ high-field point with pump between levels 1 and 3 and the $\theta = 54.7°$ point at 4.2°K and 1.6°K.

The inversion measurements were obtained by placing a single slab of ruby in the slow-wave structure, the other slabs of ruby being replaced by undoped Al_2O_3 slab. This results in more pump power being available to saturate the pump transition and yields lower gains so that regeneration effects are reduced. Enough isolation and ohmic loss were present in the structure to insure against any regeneration effects.

The inversion was measured by two different methods. The first consisted of measuring the paramagnetic absorption in db with the pump off, and the change in absorption with the pump on. I may then be computed as

$$I = \frac{\Delta \text{ db (pump off/on)} - \Delta \text{ db (P.M. absorption)}}{\Delta \text{ db (P.M. absorption)}} \cdot \quad (11)$$

The second method consisted of displaying the normal and inverted signals on an oscilloscope by using a 60-cps magnetic field sweep. A precision attenuator is then employed to measure the power ratio between the two signals.

The results of the above measurements are shown in Table II.

TABLE II
INVERSION RATIO

θ	T	f_s(Gc)	I	Pump Levels
90°	4.2°K 1.6°K	9.22 9.24	0.24 0.24	1–3
54.7°	4.2°K 4.2°K 1.6°K	9.0 9.24 8.65	2.6 2.65 2.7	1–3 and 2–4

Eq. (7) gives the theoretical inversion at $\theta = 90°$ for equal relaxation times between all levels. This gives a value of 0.35, which is to be compared with the measured value of 0.24. The discrepancy may be attributed to an unfavorable relaxation time ratio; *i.e.*, the idler relaxation time is slightly greater than the signal relaxation time.

The inversion at the second mode of operation at the $\theta = 90°$ point (pump between levels 1 and 4) was not measured because no pump source was available in this frequency range ($\approx$43–46 Gc). Higher inversions would be expected for this mode of operation. However, high pump powers would be required to saturate the pump transition because the transition matrix elements become very small between the 1 and 4 levels at this high value of magnetic field [11].

The inversion ratio results at the $\theta = 54.7°$ point were surprisingly high[2] and thus were measured several times.

[2] In a private communication with Dr. R. W. Degrasse of the Microwave Electronics Corp., the authors were informed that he has measured inversion ratios of around 2.5 at this point of operation.

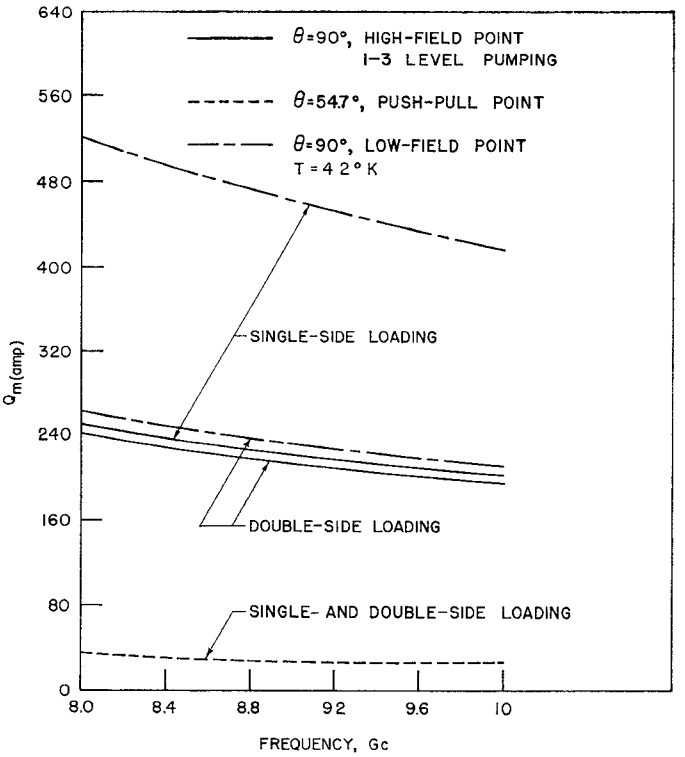

Fig. 6—$Q_{m(\text{amp.})}$ vs frequency for single- and double-side loading at different operating points for circularly polarized RF fields.

Enough isolation was incorporated in the structure to suppress regeneration effects. The theoretical inversion ratio for equal relaxation times between all levels is approximately equal to 1.64. It was shown, however, in (9), that for the ideal case ($w_{41} = \infty$) the inversion could be as high as 4.3 at this point. Thus the measured inversion of 2.7 is certainly within the theoretical limits. It can be seen from (8) that for $w_{21} = w_{32} = w_{43} = w$, an inversion ratio of 2.7 may be obtained for $w_{41}/w \cong 3.66$.

The gain in the maser, (1), is inversely proportional to the amplification magnetic $Q[Q_{m(\text{amp})}]$, where

$$Q_{m(\text{amp})} \triangleq \frac{Q_{m(\text{abs.})}}{I} \cdot \quad (12)$$

This quantity is plotted in Fig. 6 as a function of frequency for circularly polarized RF fields.

It is seen that operation at the push-pull point is far superior to operation at either of the other points.

III. Traveling-Wave Maser Experimental Results

Cross sections of the traveling-wave maser are shown in Fig. 1. An assembly of the maser and the scheme of coupling the signal and the pump into the structure are shown elsewhere [5]. The active length of the structure that was employed in these experiments is approximately 1.8 inches. The structure was loaded with four ruby slabs as shown in Fig. 1. A YIG slab for providing the necessary isolation was placed in the structure and

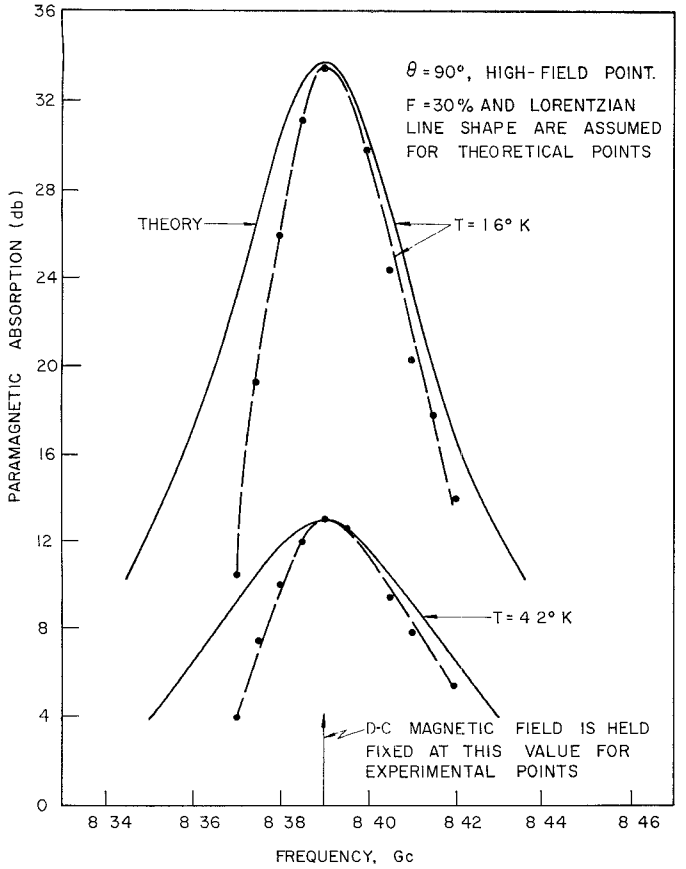

Fig. 7—Paramagnetic absorption in the traveling wave maser. (Active structure length = 1.8 inches.)

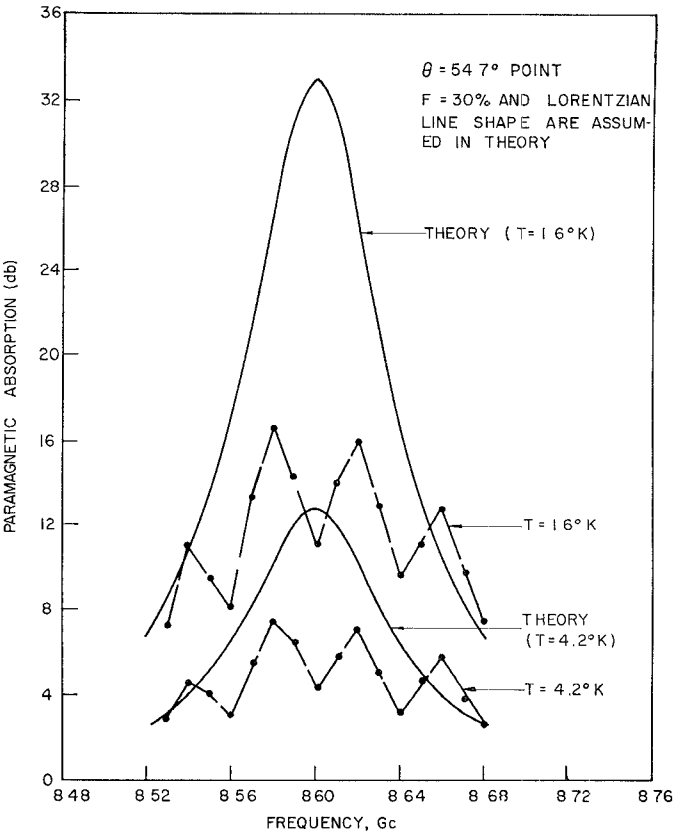

Fig. 8—Paramagnetic absorption in the traveling-wave maser. (Active structure length = 1.8 inches.)

its location is also shown in Fig. 1. The pass band of the structure was approximately 900-Mc wide and the slowing factor across the band is shown in Fig. 2.

A. Paramagnetic Absorption Measurements

The paramagnetic absorption was measured at the $\theta = 90°$ and 54.7° points. This is shown in Figs. 7 and 8 where it is compared with the expected theoretical absorption.

At the $\theta = 90°$ point the c axes of the ruby slabs are well aligned. Since this is a turning point where the magnetic field varies slightly with the angle θ at a particular frequency, small variations of the c axis along the crystal will thus have little effect on the paramagnetic absorption. It is seen that at this angle an assumed filling factor of 30 per cent gives good agreement between the experimental results and the theoretical predictions.

For a filling factor of 30 per cent, which was chosen to fit the experimental results at the $\theta = 90°$ point, the paramagnetic absorption at the $\theta = 54.7°$ point may be predicted. The predicted absorption and the experimental measurements are shown in Fig. 8. The discrepancy between the theoretical and experimental results may be attributed to either or both of two different factors. The first is due to χ' and the second is due to the nonuniformity of the c axis in the ruby slabs and to the misalignment of the slabs in the structure. χ' varies rapidly [1] in the vicinity of the resonance region and thus may introduce some perturbation in the $\omega - \beta$ characteristic which may result in the discrepancy in the absorption as shown in the figure. The variation of χ' may also change the input and output coupling of the signal power from its value when the dc magnetic field is off since this essentially changes the input and output impedance match and thus may lead to measured values which are lower or higher than the actual absorption. A poor impedance match, which is the case here, would tend to accentuate this effect. It should be noted here that this effect may also lead to measured inversion ratios which are slightly higher than the actual ones. The c-axis variation is more critical at this point than at the $\theta = 90°$ point, and thus any small variation in the c axis along the ruby slab would have a greater effect at this operating point. Due to the nonuniformity of the c axes, it is seen that the absorption occurs over a wider frequency range and of coursed the measured absorption would be smaller than the predicted one which assumes a single line. It is believed that this problem can be circumvented, however, by utilizing more uniform crystals.

B. Gain Measurements in the Traveling-Wave Maser

Electronic gain measurements were performed at the $\theta = 54.7°$ and 90° high-field points. A YIG slab whose characteristics are discussed in a later section was incorporated in the structure to provide the necessary isolation and insure against any regenerative effects.

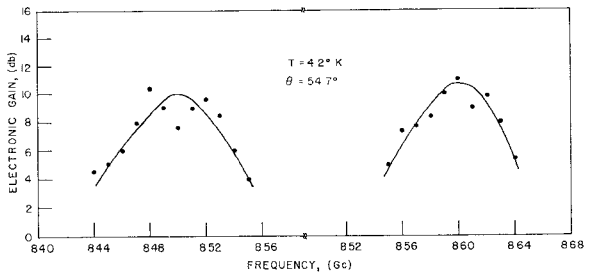

Fig. 9—Electronic gain in the traveling-wave maser. (Active length = 1.8 inches.)

At the $\theta = 90°$ point the pump power was applied between levels 1 and 3. It was found that the available pump power was not sufficient to obtain any inversion at this point. The pump power available was just sufficient to saturate the signal transition but not enough to produce any inversion. The inversion ratio at this point was measured, however (Section II-B, 4), and thus the obtainable gain with enough pump power may be predicted. There was no source of power available to investigate the second mode of operation at this point, *i.e.*, pump between levels 1 and 4. This mode of operation should yield a higher inversion ratio and thus more gain in the maser.

The measured electronic gain at $\theta = 54.7°$ and $T = 4.2°$K is shown in Fig. 9. The backward loss of the YIG isolator at these points was on the order of 15 to 20 db. The irregularities in the gain curve are believed to be due to the same effects that produce the irregularities in the absorption curve and were discussed in the previous section. One additional factor which contributes to this effect is the χ' of the YIG slab in this case, which is possibly the reason that the gain curves do not show as pronounced a variation as the absorption curve. Since the measured inversion ratio at this point is approximately 2.6 (Section II-B, 4) a higher electronic gain than that obtained was expected. The reason for the lower gain was the lack of pump power which was insufficient to completely saturate the pump transitions.

At this point upon reducing the temperature to 1.6°K the maser broke into oscillation. This was due to the lack of isolation provided by the YIG slab.

The preceding experimental results indicate that with good, well aligned ruby crystals, a well-matched structure, and sufficient pump power to saturate the pump transitions, excellent agreement between the experimental results and the theory would result. For such a case, the expected electronic gain which would be obtained in this 1.8-inch-long structure is shown in Fig. 10.

The instantaneous bandwidth of the maser where a Lorentzian line shape is assumed may be expressed as [1],

$$B = B_m \sqrt{\frac{3}{G_{\text{db}} - 3}} \tag{13}$$

where B_m is the linewidth of the signal transition.

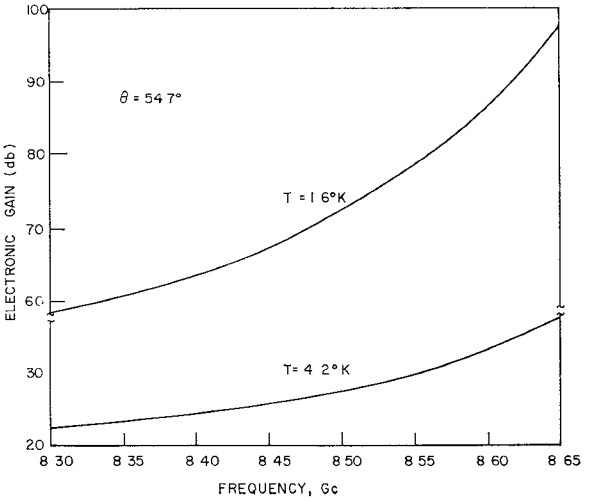

Fig. 10—Expected electronic gain in the traveling-wave maser with good, well aligned crystals, good impedance match and sufficient pump power. (Active maser length = 1.8 inches.)

IV. Isolators

The isolator material which was employed in these experiments is polycrystalline yttrium-iron-garnet (YIG). The isolator was in the form of long slabs. The aspect ratio of the slab may be chosen to yield the required resonance frequency for tracking the ruby resonance. The resonance frequency may be expressed in general as [14]

$$f_r(\text{mc}) = \gamma\{[H_z - (N_z - N_x)4\pi M_s] \cdot [H_z - (N_z - N_y)4\pi M_s]\}^{1/2} \tag{14}$$

where

f_r = the resonance frequency
γ = gyromagnetic ratio = 2.8 Mc/gauss
H_z = applied dc magnetic field, gauss
N = demagnetization factor
$4\pi M_s$ = saturation magnetization, gauss.

For a long rectangular slab as shown in Fig. 11, the demagnetization factors may be written approximately as [15]

$$N_x = 0$$
$$N_y = \frac{a}{a + b}$$
$$N_z = \frac{b}{a + b} \cdot \tag{15}$$

Substituting for N_x, N_y, and N_z in (16) yields

$$f_r = \gamma\left\{\left[H_{\text{dc}} - \left(\frac{\alpha}{1 + \alpha}\right)4\pi M_s\right] \cdot \left[H_{\text{dc}} + \frac{(1 - \alpha)}{(1 + \alpha)}4\pi M_s\right]\right\}^{1/2} \tag{16}$$

where $\alpha = b/a$ = the aspect ratio.

For YIG, $4\pi M_s = 1750$ gauss at room temperature and 2480 gauss at 4.2°K[2].

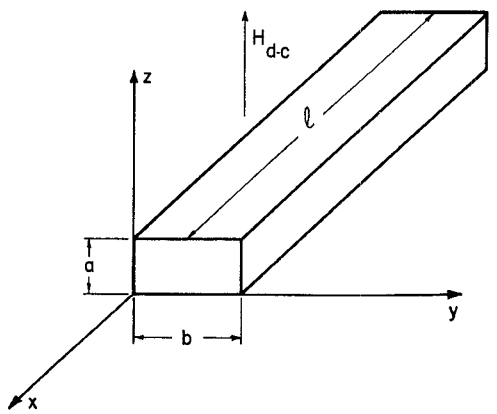

Fig. 11—Dimensions and orientation of a YIG slab. ($l \gg a$ or b.)

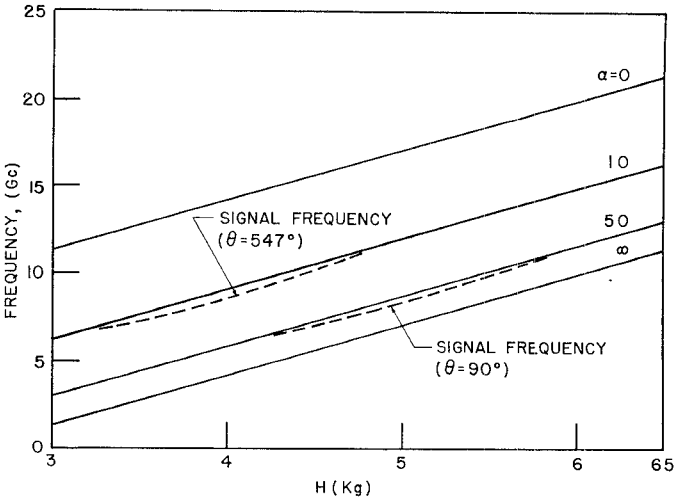

Fig. 12—Resonance frequency of YIG slab at 4.2°K and ruby signal frequency vs magnetic field.

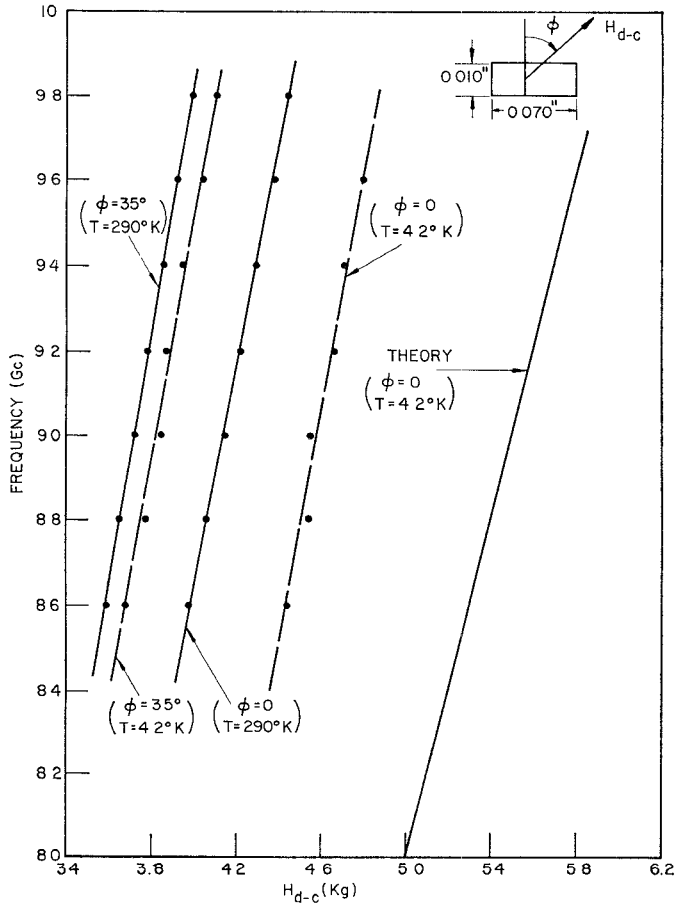

Fig. 13—Resonance frequency of a YIG slab.

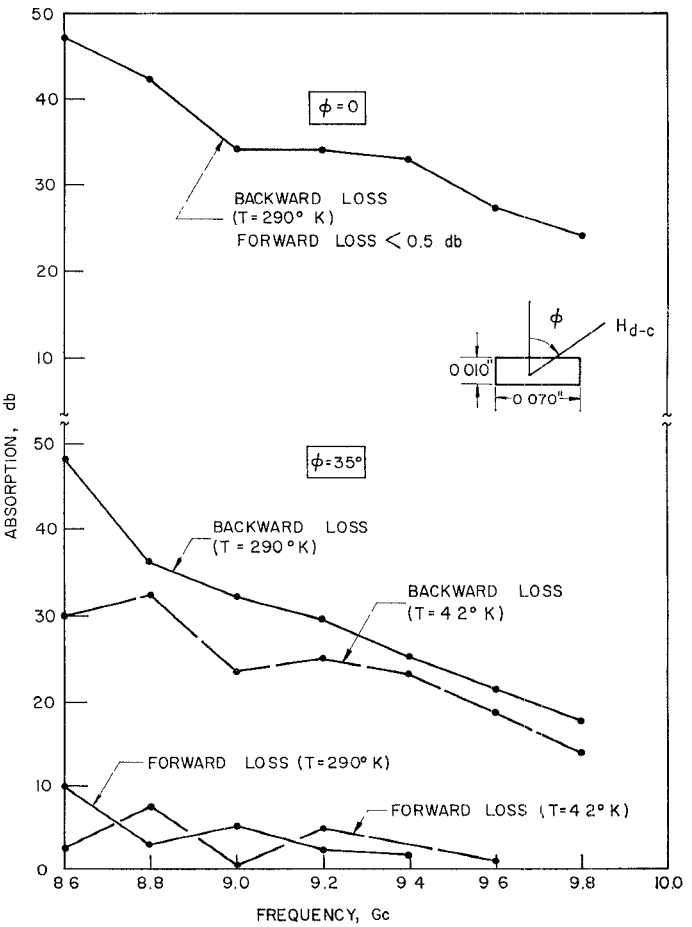

Fig. 14—Backward and forward absorption of YIG slab isolator. (Length = 1.8 inches.)

The resonance frequency of a YIG slab is shown in Fig. 12 for different aspect ratios. The bounding curves, $\alpha=0$ and $\alpha=\infty$, are exact and they give the limits over which the resonance frequency may be varied. The resonance frequency of the ruby signal transition at $\theta=90°$ and 54.7° is also shown in Fig. 12. It is seen from this figure that a YIG slab may be shaped to have a resonant frequency which coincides with the ruby signal frequency.

A YIG slab 0.01 inch by 0.070 inch was cut and placed in a slow-wave structure whose pass band was approximately 2 Gc wide in order to measure the resonance frequency as a function of the magnetic field. The results are shown in Fig. 13 for two different orientations of the magnetic field relative to the broad face of the ferrite. These would correspond to the $\theta=90°$ and 54.7° points in ruby if the slab is located in the structure as shown in Fig. 1.

For the $\phi=0$ case, *i.e.*, the magnetic field perpendicular to the broad face of the ferrite, several resonance lines were observed and adequate absorption was obtainable over a 1 kilogauss band. It can be seen from the figure that the resonance frequency changes with the angle ϕ at a constant magnetic field. This is another method of changing the resonance frequency without changing the aspect ratio. This method may prove useful in certain applications. It was employed in the traveling-wave maser experiments to make the ferromagnetic resonance and the ruby signal frequency resonance coincide. This was achieved by tilting slightly the ferrite slab shown in Fig. 1 about the z axis.

The forward and backward absorptions in a slab 1.8 inches long placed in a structure with a pass band of 2 Gc (8–10 Gc) are shown in Fig. 14. This slab was also used in the traveling-wave maser which was discussed in the previous section. For the $\theta=90°$ point of ruby and the ferrite placed in the structure as shown in Fig. 1, a backward loss of approximately 25 db at 4.2°K and a forward loss of approximately 1 db and less were obtained at the maser operating points. For the $\theta=54.7°$ point in ruby the ferrite sab was tilted slightly about the z axis from the position shown in Fig. 1 in order to make the resonant frequency of the YIG slab and the ruby signal frequency coincide. For this case a backward loss of approximately 20 db and a forward loss of 1 db and less were obtained at the maser operating points and at 4.2°K.

V. Conclusions

It may be concluded that the $\theta=54.7°$ point is far superior to the other points considered here for traveling-wave maser operation at X band. With good single crystals, good impedance match of the signal power in and out of the structure and sufficient pump power, all of which can be achieved, electronic gains in the neighborhood of 15 db per inch at 4.2°K and 40 db per inch at 1.6°K can be obtained. The gain at this point is very sensitive to c-axis deviation of the ruby crystals. C-axis deviations of greater than 0.25° over the length of the maser will have a considerable effect on the gain. The c-axis deviation is not as severe at the $\theta=90°$ point, but the inversion ratio using a pump between levels 1 and 3 is very low and thus very little gain results. However, pumping between levels 1 and 4 will enhance the inversion and would then result in adequate gain. The inversion ratio using a 1 to 4 pump at this point was not measured because no source was available at this frequency.

YIG slabs have been shown to yield adequate absorption for isolation purposes. More isolation may be obtained by utilizing more than one slab if so desired. It was shown that the resonance frequency of a YIG slab may be varied by changing the orientation of the slab relative to the dc magnetic field. This might prove useful in certain applications where a higher resonance frequency may be required at a particular dc magnetic field which may not be obtained by an aspect ratio variation.

Acknowledgment

The authors gratefully acknowledge the discussion with Prof. J. E. Rowe concerning this work.

References

[1] R. W. Degrasse, E. O. Schulz-Dubois, and H. E. D. Scovil, "The three-level solid state traveling-wave maser," *Bell Sys. Tech. J.*, vol. 38, pp. 305–335; March, 1959.
[2] S. Okwit and J. G. Smith, "Packaged electronically tunable S-band traveling-wave maser system," Proc. IRE, vol. 50, pp. 1470–1483; June, 1962.
[3] W. S. C. Chang, J. Cromack, and A. E. Siegman, "Cavity and Traveling-Wave Masers Using Ruby at S-Band," 1959 IRE WESCON Convention Record, pt. I, pp. 142–150.
[4] H. B. Yin, L. C. Morris, and D. J. Miller, "An S-band traveling-wave maser," Proc. IEEE (*Correspondence*), vol. 51, p. 225; January, 1963.
[5] G. I. Haddad and J. E. Rowe, "X-Band ladder-line traveling-wave maser," IRE Trans. on Microwave Theory and Techniques, vol. MTT-10, pp. 3–8; January, 1962.
[6] F. E. Goodwin, J. E. Kiefer, and G. E. Moss, "The Coupled-Cavity Transmission Masers—Engineering Design," Hughes Research Laboratories, Jackson, Miss., Research Rept. No. 252; October, 1962.
[7] F. Arams and B. Peyton, "Tunable millimeter traveling-wave maser operation," Proc. IRE (*Correspondence*), vol. 50, pp. 1647–1698; July, 1962.
[8] G. I. Haddad, "Dielectrically-Loaded Ladder Lines for Traveling-Wave Maser and Other Applications," Electron Physics Laboratory, Electrical Engineering Dept., The University of Michigan, Ann Arbor, Tech. Rept. No. 65; December, 1963.
[9] C. Kikuchi, J. Lambe, G. Makhov, and R. W. Terhune, "Ruby as a maser material," *J. Appl. Phys.*, vol. 30, p. 1061; July, 1959.
[10] F. R. Abrams, "Maser operation at signal frequencies higher than pump frequency," IRE Trans. on Microwave Theory and Techniques, vol. MTT-9, pp. 68–72; January, 1961
[11] W. S. Chang and A. E. Siegman, "Characteristics of Ruby for Maser Applications," Electron Devices Laboratory, Stanford University, Calif., Tech. Rept. No. 156-2; September, 1958.
[12] T. Maiman, "Temperature and Concentration Effects in a Ruby Maser," in Quantum Electronics Symposium," C. H. Townes, Ed., Columbia University Press, New York, N. Y., pp. 324–332; 1960.
[13] A. A. Manenkov and V. B. Federov, "Investigation of the linewidth and shape in the paramagnetic resonance spectrum of the Cr^{3+} ion in corrundum single crystals," *Sov. Phys. (JETP)*, vol. 11, pp. 751–754; October, 1960.
[14] C. Kittel, "On the theory of ferromagnetic resonance absorption," *Phys. Rev.*, vol. 73, pp. 151–161; January, 1948.
[15] F. W. Ostermeyer, "Behavior of Resonance Isolators at Liquid Helium Temperature," M. S. thesis, Mass. Inst. of Tech., Cambridge; June, 1959.